Evaluating Nanoparticle Sensor Design for Intracellular pH Measurements

Rikke V. Benjaminsen, Honghao Sun, Jonas R. Henriksen, Nynne M. Christensen, Kristoffer Almdal, and Thomas L. Andresen*

DTU Nanotech, Department of Micro- and Nanotechnology, Technical University of Denmark, Building 423, 2800 Lyngby, Denmark

ABSTRACT Particle-based nanosensors have over the past decade been designed for optical fluorescent-based ratiometric measurements of pH in living cells. However, quantitative and time-resolved intracellular measurements of pH in endosomes and lysosomes using particle nanosensors are challenging, and there is a need to improve measurement methodology. In the present paper, we have successfully carried out time-resolved pH measurements in endosomes and lysosomes in living cells using nanoparticle sensors and show the importance of sensor choice for successful quantification. We have studied two nanoparticle-based sensor systems that are internalized by endocytosis and elucidated important factors in nanosensor design that should be considered in future development of new sensors. From our experiments it is clear that it is highly important to use sensors that have a broad measurement range, as erroneous quantification of pH is an unfortunate result when measuring pH too close to the limit of the sensitive range of the sensors. Triple-labeled nanosensors with a pH measurement range of 3.2–7.0, which was synthesized by adding two pH-sensitive fluorophores with different pK_a to each sensor, seem to be a solution to some of the earlier problems found when measuring pH in the endosome–lysosome pathway.

KEYWORDS: nanosensors · pH measurements · intracellular · nanoparticles · endosome · lysosome · fluorescence microscopy

Intracellular pH plays a pivotal role in cellular processes and is highly regulated in every organelle.[1] The structural stability and function of proteins are tightly associated with pH;[2] for example, it has been shown that mutations in the Vacuolar-type H^+-ATPase (V-ATPase), responsible for acidification of the Golgi compartment, results in impaired glycosylation of proteins.[3] Furthermore, cell cycle progression and programmed cell death have both been linked to changes in intracellular pH.[4,5] Thus, quantification of pH fluctuations in organelles of living cells is essential for increasing our understanding of cellular processes. Another area where an increased understanding of the pH profile in the ensosome–lysosome pathway is highly important is related to design of pH-sensitive drug delivery systems.[6] A number of nanoparticle-based pH-sensitive drug delivery systems are being reported every year where various surface ligands, *e.g.*, folate and antibodies, are attached to the surface of nanoparticles for targeting overexpressed receptors.[6,7] However, there is very limited knowledge on the intracellular trafficking of these systems, particularly regarding the pH that the particles are experiencing after internalization. At present, it is just assumed that the pH-sensitive drug delivery system ends up in acidic compartments, but this has not been tested, and it is reasonable to hypothesize that the targeting ligands used could have an effect on trafficking. Thus, nanoparticle pH sensors could play an important role in enhancing our knowledge on how different targeting ligands affect trafficking of nanoparticles in cells, which could further improve our understanding of how to design better drug delivery systems that release their cargo in a controlled manner as a response to acidification in the surroundings. Unfortunately, the methodologies for conducting measurements of pH in the endosomes and lysosomes using nanoparticle-based pH sensors are not well developed. Thus, we here focus on developing the necessary methodology and furthermore evaluate nanoparticle sensor design, which will allow us to improve the sensor systems for these types of measurements in the future.

A general limitation with fluorescence-based pH measurements is the concentration range the sensor covers. This range depends on the acid dissociation constant (K_a) of the pH-sensitive fluorophore, which gives a sigmoidal calibration curve in a pH range of the p$K_a \pm 1$, as a rule of thumb, with a nonlinear relationship between fluorescence ratio and pH. Several investigations have been made on the endosomal–lysosomal system[8−10] using particle sensors with a maximum range of two pH units. Thus, it is evident that at some point the actual pH will fall outside the range of the sensor since the pH differs by more than 2 pH units between early endosomes and lysosomes. The calibration curve can in principle provide pH values that are more than one pH unit from the pK_a value;

* Address correspondence to Thomas.andresen@nanotech.dtu.dk.

Received for review May 4, 2011 and accepted June 27, 2011.

Published online June 27, 2011
10.1021/nn201643f

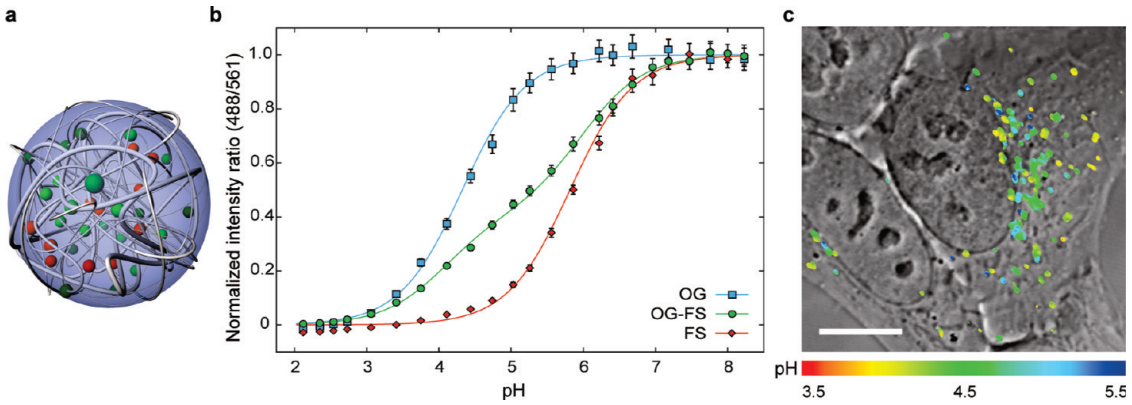

Figure 1. The triple-labeled nanosensor: design, calibration, and pH measurements. (a) Schematic of the cross-linked polyacrylamide nanoparticle. (b) *In vitro* calibration of the triple-labeled sensor with both OG and FS, and two dual-labeled sensors with either OG or FS. Normalization of ratios has been performed by subtraction of R_{min} and division by ($R_{max} - R_{min}$) for all sensors in relation to their respective fitted calibration curve. Mean ± SD between 450 regions of interest (ROIs) are presented. (c) Uptake of the triple-labeled sensor by a HepG2 cell after 24 h and washing and imaged with confocal microscopy. A combined image where the ratios from the intensity images are converted into pH *via* the calibration curve and color coded on a linear scale according to pH, thereafter overlaid with the differential interference contrast (DIC) image. Scale bar, 10 μm. OG = Oregon Green; FS = fluorescein.

however, these measurements are sensitive to even the smallest errors due to sensor fluorophore saturation,[11−14] and such measurements can give misleading results. In addition, as we will show in this report, it is problematic to do reliable quantification of the pH close to the sensor's range limit. The calibration curves have been the Achilles heel in many studies, and even though it is the most important part of a quantitative study of pH in cells, it is often carried out in an inappropriate way or even not presented, thereby precluding the possibility of data evaluation.[15−17] Finally, localization of the sensor inside the cell is essential in order to evaluate and understand the measurements,[18] and failure to do so can lead to misinterpretation of results. Many of these considerations are also important in the quantification of other metabolites in cells.[19−24]

During the past two decades numerous optical nanoparticle-based sensors (nanosensors), dual-labeled with a pH-sensitive and an insensitive fluorophore for ratiometric measurements, have been developed and are well designed from a synthetic point of view.[25−29] These nanosensors have overcome many of the problems encountered when cells are loaded with free dye;[29−31] however, lack of sensor evaluation in a biological setting has precluded the realization of the fact that earlier developed dual-labeled nanosensors are too limited in their pH sensitivity range to be useful in cellular measurements in the endosome−lysosome pathway. In a series of cellular experiments we have found that previous dual-labeled sensors can give misleading results. This problem has actually been pointed out by Downey *et al.*[32] more than 10 years ago, where they studied the pH in phagocytic cells using fluorescent-labeled zymosan and provided important insight into the challenges associated with pH measurements. We show here that recently reported nanometer-sized polymeric particle sensors, triple-labeled with a dynamic measurement range of almost 4 pH units[33] that covers the entire physiologically relevant range of the endosome−lysosome pathway, provide reliable results. We demonstrate the application of this sensor in real-time pH measurements in living cells and show the importance of its design relative to earlier reported sensor types.[34] Furthermore, we provide an equation describing the calibration curve of this triple-labeled sensor derived from thermodynamic principles, along with an in-depth description of how to analyze and evaluate ratiometric images.

RESULTS

Design and Principle of Triple-Labeled Nanosensor. We have investigated a nanoparticle-based optical sensor with two sensor dyes and a reference dye for ratiometric measurements utilizing an acrylamide cross-linked matrix. This matrix constitutes a porous nanoparticle (Figure 1a) that protects the sensor dyes from interferences in the cell as earlier reported,[35] with a very fast response time to changes in pH and full control over dye ratios during measurement. The two pH-sensitive fluorophores that are covalently attached to the particle are Oregon Green (OG) and fluorescein (FS), along with the pH-insensitive rhodamine B (RhB) (for synthetic procedure see Supporting Information). When incorporated into the employed particle matrix, the pK_a values of Oregon Green and fluorescein are 4.1 and 6.0, respectively (found as fitting parameters to the calibration curve). This gives a small overlap in their pH measurable ranges and results in a doubling of the measurable pH range in comparison to sensors with one sensitive fluorophore.[34] Oregon Green and fluorescein are both excited at 488 nm and show identical emission spectra, but their intensity dependency on pH is not the same, which is easily realized by their

differences in pK_a. Furthermore, when used as covalently bound sensor fluorophores in nanosensors, their ratio has to be optimized to obtain optimal ratiometric curves. Figure 1b shows ratiometric curves, measured on the microscope, of calibration emission spectra between the sensor and reference fluorophores in the nanoparticle sensors, excited at 488 and 561 nm, respectively, as a function of pH. Two dual-labeled sensors with FS or OG and the recently reported[33] triple-labeled sensor (FS and OG in the same nanoparticle) are shown (all with rhodamine B as the reference fluorophore).

The dual-labeled sensors follow a sigmoidal function described by

$$R = \frac{R_1}{10^{pKa - pH} + 1} + R_0 \quad (1)$$

where R is the ratio of emission intensities excited at 488 and 561 nm, $R_0 = R_{min}$ (the ratio for the fully protonated form), $(R_1 + R_0) = R_{max}$ (the ratio for the fully deprotonated form), and pK_a is the specific pK_a value for the fluorophore when incorporated into the particle. This equation is in accordance with what has previously been derived for transcribed GFP-based pH indicators.[23] In this field of transcribed pH sensors important considerations on derivation of calibration curves and actual pH measurements have been published.[36,37] The triple-labeled sensor follows an extended version of eq 1:

$$R = \frac{R_1}{10^{pKa_1 - pH} + 1} + \frac{R_2}{10^{pKa_2 - pH} + 1} + R_0 \quad (2)$$

where $R_0 = R_{min}$, $(R_1 + R_2 + R_0) = R_{max}$, and pK_{a1} and pK_{a2} are the specific pK_a values of the two pH-sensitive fluorophores when incorporated into this particle, here fluorescein and Oregon Green. The calibration curves have been normalized according to their fitted equations by subtraction of R_{min} and division by $(R_{max} - R_{min})$. Methods for calculating pH as a function of R are presented in the Supporting Information (supporting eqs S1 and S2), along with a more thorough description of the derivation of a more generalized form of eqs 1 and 2 (supporting eq S3).

The triple-labeled sensor has a very large dynamic range, with a 13.5-fold increase in ratio from pH 3.2 to 7.0. This makes it very suitable for measurements in the endosomal–lysosomal pathway. The developed sensor is spontaneously taken up by HepG2 cells *via* endocytosis due to the surface chemistry of the sensor (being weakly cationic), and after 24 h they reside in compartments with a pH of 4.5 ± 0.4 (mean ± standard deviation (SD)) (Figure 1c). With the new sensor even large changes in pH in both directions can now be reliably measured. All measurements of pH were performed after subtraction of background in each channel. The background of every image series was determined from a histogram of all pixels (Supporting Figure S1). Further image analysis was performed by two methods, either based on regions of interest (ROIs) utilizing the Fiji processing package based on ImageJ[38] or with a pixel by pixel method based on custom-made software, both described in the Methods section. The two methods give identical results, and a comparison can be found in Supporting Figure S2. The pixel-based method allows us to generate corresponding pH images by mapping the ratio of each pixel onto a linear pH color scale, which was combined with differential interference contrast (DIC) images to produce overlay images (*e.g.*, Figure 1c).

pH-Sensing Capabilities of the Triple-Labeled Sensor. During maturation of endosomes to lysosomes there is a characteristic decrease in pH, which is driven by the V-ATPase proton pump.[39] Bafilomycin A_1 is a specific inhibitor of V-ATPases[40,41] and has been shown to inhibit the acidification of phagosomes,[32] but also a study on the accumulation of the acidotropic weak base acridine-orange in acidic compartments has indicated that it increases the pH of endosomes and lysosomes.[42] Figure 2a (top panel) shows the uptake of the triple-labeled sensor after 24 h, before and after treatment with bafilomycin A_1. This sensor shows a profound shift in pH, which is illustrated as a color change from yellow-green to a more blue color after 30 min. The histogram in Figure 2b also reveals that the pH does indeed increase more than 1 pH unit from having a maximum at pH 4.3 to 5.6. Inhibition as a function of time with cell measurements at 5 min intervals shows a steady increase in pH up to 30 min (Supporting Figure S3). This pH range lies well within the boundaries of the pH sensitivity of the triple-labeled sensor, thereby giving reliable and accurate measurements. In order to exclude that the change in pH was caused by differential photobleaching of the fluorophores, control experiments were performed; cells with internalized nanosensor were imaged continuously for more than seven images. This experiment showed no alterations in pH between the seven images, showing that it is the treatment with bafilomycin A_1 that is causing the increase in pH. Furthermore, as it is the pH-sensitive fluorescein derivatives that are least photostable (easily observed by increasing laser power), a decrease in ratio would be the consequence, hence a decrease in pH.

Erroneous pH Measurements with a Conventional Dual-Labeled Sensor. Unreliable results are obtained when making the same measurements as described above with a conventional dual-labeled sensor with a pK_a value of 4.3. Figure 2a (middle panel) shows the uptake of the dual-labeled sensor with Oregon Green as the pH-sensitive fluorophore after 24 h. Images were taken before and after treatment with bafilomycin A_1 for 30 min, and the color bar used for the pH scale is the same as applied for the triple-labeled sensor (Figure 2a top panel). The corresponding pH histograms are shown in Figure 2c. With a pK_a value of 4.3 the measurable range

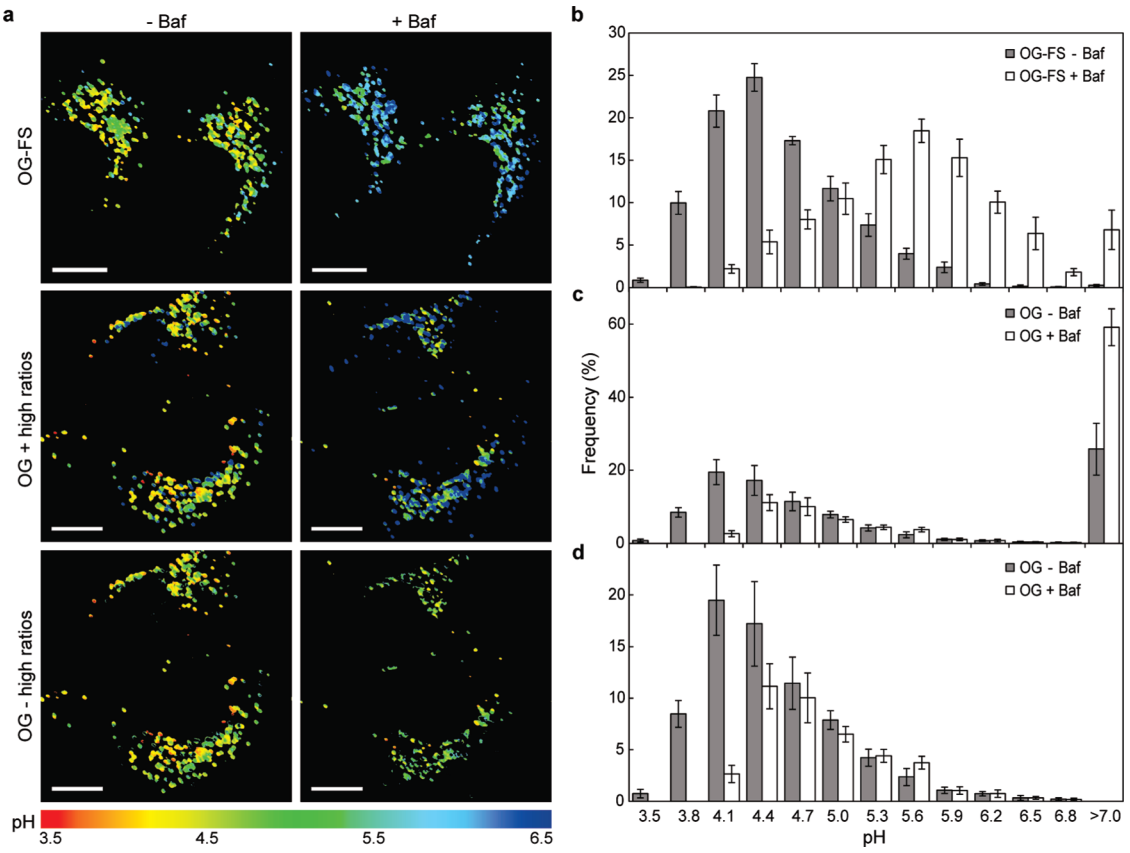

Figure 2. Measurements of pH changes of more than 1.1 pH units. (a) Nanosensor internalized during 24 h by HepG2 cells imaged by confocal microscopy before and after treatment with bafilomycin A_1 for 30 min. The ratio of the pH-sensitive and reference fluorophores was converted into pH *via* the respective calibration curve and color coded on a common linear scale according to pH. Top: triple-labeled sensor. Middle: Dual-labeled nanosensor with pK_a value of 4.3, including pixels yielding ratios larger than R_{max} in blue. Bottom: Same as middle, without pixels with ratios larger than R_{max}. Scale bars, 10 μm. (b, c, and d) Histograms showing pH distribution of nanosensor-containing vesicles of the cells in (a) respectively, before and after bafilomycin A_1 treatment. The pH axis of the histograms corresponds to the sensitivity range of the triple-labeled sensor. Bottom histogram is a magnification of the middle histogram excluding measurements with a ratio larger than R_{max}. Mean ± standard error of the mean (SEM) (n = 8 and 5 images for triple and dual-labeled nanosensors, respectively) are presented, and at least 1400 ROIs were analyzed for each treatment. The presented data are representative of six and three independent experiments for the triple and dual-labeled nanosensors, respectively. OG = Oregon Green; FS = fluorescein; Baf = bafilomycin A_1.

of this sensor covers the interval 3.4−5.2. If the actual pH exceeds these limits by a small margin, the sensor will still return pH values; however, these values will be outside the range where quantitative measurements are possible due to the sigmodial shape of the calibration curve, *i.e.*, at the plateaus where small changes in the ratios correspond to large changes in pH. Thus, the measurements are sensitive to even the smallest errors and are unreliable. For the dual-labeled sensor, the total amount of pH values measured that exceed pH 5.2 and thus fall outside the range where measurements are reliable is ∼34% and 70% before and after treatment with bafilomycin A_1, respectively (see also Figure 3). One should therefore always present data in histograms where the fraction that is outside the measurement range is indicated; for example, for the triple-labeled sensor, Figure 2b shows the measurable range (3.2−7.0) together with all measurements exceeding this, presented as >7.0. Furthermore, when presenting the histogram of the dual-labeled sensor on the same pH scale (for simplicity) as the triple-labeled sensor (Figure 2c), the result is a presentation of unreliable pH measurements in the range 5.3−7.0 (where the measurement is at the plateau of the sigmoidal standard curve), and values above are represented by >7.0. All pixels with a pH value exceeding 7.0 are in the middle panel of Figure 2a represented by a blue color. Choosing to ignore these values and zooming in on the pixels that are in the measurable range of the sensor results in the histogram shown in Figure 2d, with the corresponding pH images in the bottom panel of Figure 2a, where the blue pixels with high ratios have been removed. The remaining pixels show only a very slight change in color, implying that the pH rises minimally after the treatment. The histogram of pH in Figure 2d reveals a maximum at pH 4.2 before treatment with bafilomycin A_1 and at pH 4.4 after the treatment. Thus, the histogram leads to the erroneous conclusion that the pH shows only a very slight change after treatment with bafilomycin A_1.

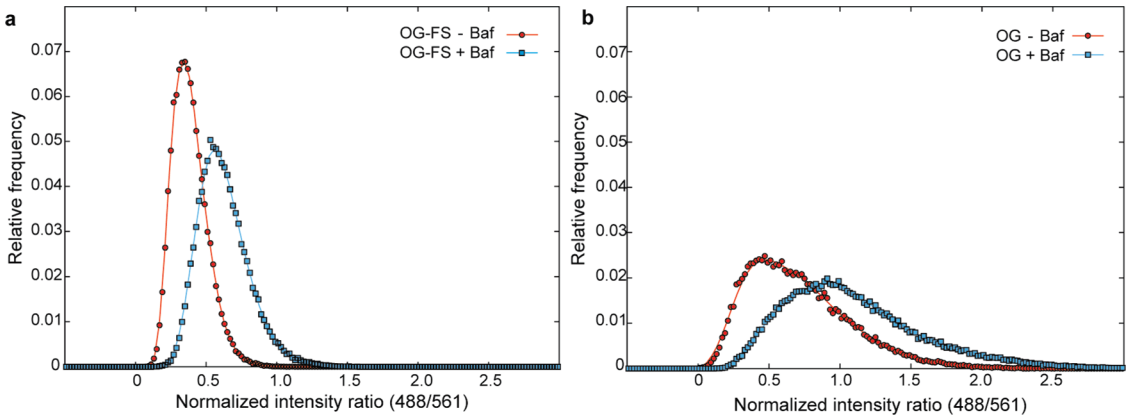

Figure 3. Distributions of ratios determined using a pixel-by-pixel image analysis of cells with internalized nanosensors before and after treatment with bafilomycin A_1. (a) Triple-labeled sensor and (b) dual-labeled sensor. The presented data are representative of six and three independent experiments for the triple and dual-labeled nanosensors, respectively. The maximum relative error in each data point is 7%.

Distribution of Ratios within a Measurement. The distribution of pH measured in a cell is determined by the distribution of ratios. Figure 3 shows the distribution of ratios corresponding to the pH histograms presented in Figure 2 for the triple and dual-labeled sensors before and after treatment with bafilomycin A_1. The ratio is normalized in order for the full range of the sensor to cover the interval 0 to 1, where $R_{max} = 1$. From the distribution of ratios it can be seen that the change in the main ratio is larger for the dual-labeled sensor than for the triple-labeled sensor. However, as the pH interval covered by the triple-labeled sensor is larger, the ratio interval from 0 to 1 also represents a larger pH interval for the triple-labeled sensor than for the dual-labeled; hence the same change in ratio corresponds to a larger pH change for the triple-labeled sensor. What is also evident from the distributions of ratios for the dual-labeled sensor is that both distributions exceed R_{max} (=1), and it is therefore not possible to determine the exact pH of these measurements. This is especially pronounced after treatment with bafilomycin A_1, where the maximum of the distribution resides at 1, leaving about 50% of the measurements above R_{max} in the presented data set, indicating that the true pH is larger than the upper limit of the dual-labeled sensor. The true pH, as measured with the triple-labeled sensor seen in Figure 2b, indeed has a maximum around pH 5.6 and covers a broad range from 4.1 to 7.1. As the majority of this distribution of pH exceeds the measurement range of the dual-labeled sensor (3.4−5.2), it is evident that the distribution of the ratios will be situated around R_{max}, and measurements exceeding this cannot not be reported as a specific pH but rather as being larger than a certain pH, as illustrated in Figure 2c. To circumvent this problem, one should utilize sensors that have a measurement range wide enough to measure all pH values in the cell, such as the triple-labeled sensor evaluated in this article.

Other sensors, such as magnesium,[19] calcium,[43] and zinc[24] sensors, which also rely on the binding of the metabolite the sensor is designed for, could potentially encounter the same problems.

pH Measurements in Time and Space. The triple-labeled sensor spans a pH interval that covers the whole physiologically relevant interval with respect to the endosomal−lysosomal system, and its surface chemistry furthermore ensures that it targets the lysosomes after endocytosis. It is therefore possible to study the kinetics of compartmental acidification as the endosomes mature into lysosomes. HepG2 cells were treated with the nanoparticle sensor for 1.5, 2.0, and 24 h. Images presented in Figure 4a show DIC images to the left, images with pH represented by a color bar in the middle, and to the right overlays of the two. After 1.5 h it is evident that the nanosensor particles are taken up by endocytosis, showing a distinct punctuate pattern throughout the cytoplasm of the cell. A histogram of the pH after 1.5 h of treatment shows a broad peak with a mean pH of 5.1 ± 0.6 (mean ± SD) (Figure 4b). Many particle sensors reside in endosomes, some have just been taken up and experience a high pH > 6.5, and some have already reached more acidic compartments. After 2 h the pH histogram reveals a shift toward lower pH with a mean pH of 4.9 ± 0.6 (mean ± SD). A long tail toward higher pH can still be observed, indicating that not all particles have reached an acidic compartment. After 24 h of treatment the pattern has changed to a more perinuclear location, and more particles have been taken up. At this point the pH shows a narrow peak around 4.5 ± 0.4 (mean ± SD), indicating that all nanoparticle sensors have reached a highly acidic compartment. These kinetic measurements of the acidification process reveal that the endocytosis event and successive transport to acidic compartments is a fast process, taking less than 1.5 h. Furthermore, judging from the kinetics of acidification from 1.5 to 2 h, most particles have probably reached

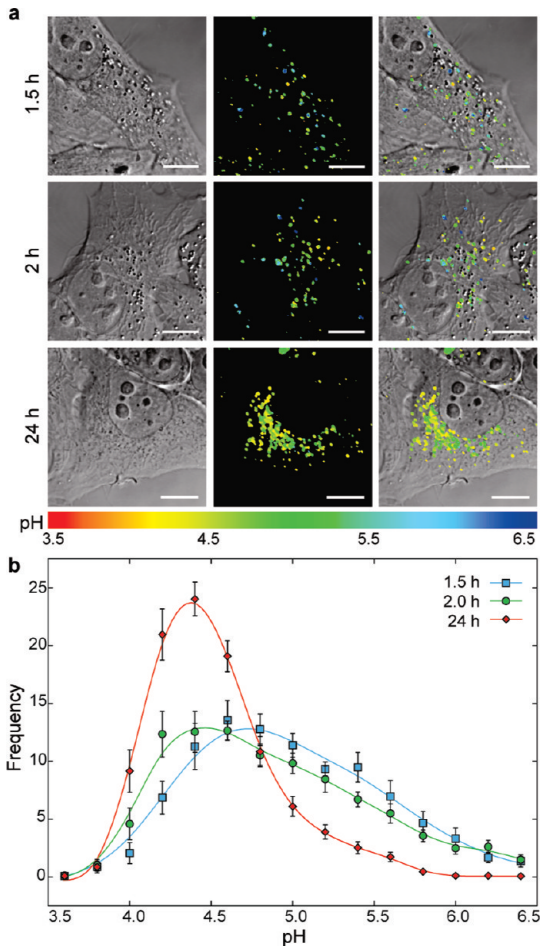

Figure 4. Kinetic studies of the uptake and acidification. (a) HepG2 cells with internalized triple-labeled nanosensor after 1.5, 2.0, and 24 h. The intensity ratios were converted to pH *via* the respective calibration curves, and all three images were color coded according to a common pH scale. Left column: DIC images; middle column: pH images; and right column: pH images overlaid with the corresponding DIC images. Scale bars, 10 μm. (b) Histogram showing pH distribution of the nanosensor-containing vesicles presented in (a). Mean $\pm$ SEM (n = 11, 13, and 23 images for 1.5, 2.0, and 24 h, respectively) with a total of ~1450, ~1800, and ~3100 nanosensor-containing vesicles analyzed.

the acidic compartments before 24 h. The pH does not decrease any further over time, indicating that the sensors have reached their final destination, potentially the lysosomes. Importantly, we still see a strong signal from both rhodamine B and the pH-sensitive fluorophores co-localizing with each other, indicating that both the fluorophores and the particles are intact at this low pH, which has also been confirmed by chemical degradation studies.

A co-localization study after 24 h between the lysosomal marker, lysosome-associated membrane protein 1 (LAMP-1),[44] and rhodamine B-labeled nanoparticles recognizes these acidic compartments as lysosomes (Figure 5a). Transient expression of LAMP-1 fused to green fluorescent protein (GFP) was obtained in HepG2 cells using BacMam viruses (recombinant baculoviruses with mammalian expression casettes).[45,46] Significant co-localization was observed with an overlap coefficient of 71% and a Pearson's correlation coefficient of 0.69,[47,48] whereas co-localization with the early endosomal marker Rab5a fused to GFP[49,50] showed no co-localization with coefficients of 26% and 0.18, respectively (Figure 5b). Similar results were obtained with a neutral nanoparticle (Supporting Figure S4), demonstrating that localization to lysosomes does not depend on the nanosensor surface charge.

Finally, we show that the nanoparticle has a very low cytotoxicity at the concentrations (10 μg/mL) utilized for these measurements, as assayed by the XTT viability assay (Supporting Figure S5).

Evaluation of the *in Vitro* Calibration Curve. Many fluorophores have been shown to change their fluorescence when interacting with proteins.[35] This has been a major problem in early intracellular pH measurement studies, and the nanoparticle-based sensor was developed to circumvent this problem. In order to evaluate whether this sensor is a reliable tool to use in a cellular environment, we developed a buffer that imitates the cytoplasm with all the components of a cell. HeLa cells were sonicated and then mixed with appropriate buffers, pH was determined, and this artificial cytoplasm was mixed with the nanosensor for preparation of a calibration curve. Furthermore, an *in situ* calibration curve was generated by ratiometric measurements in cells with internalized nanosensor incubated in K^+-rich buffers of known pH in the presence of the H^+/K^+ antiporter nigericin.[31] Both calibration curves are equivalent to a curve obtained in pure buffer (Figure 6), indicating that measurements done with this type of sensor will provide reliable results even though calibration is done in a buffer system. Calibration can be even further simplified, as our results show that all calibration curves done on different days and with different microscope settings can be superimposed when normalized. Normalization was done by subtracting with R_{min} followed by division with ($R_{max} - R_{min}$) for all ratios (Supporting Figure S6). Calibration can then be reduced to only two measurements in buffer at two different pH's (depending on desired accuracy), which is imaged with the same microscope settings as used for the corresponding cell measurements, thereby correcting for day-to-day variations and differences in microscope settings.

DISCUSSION

We have carried out the first biological evaluation of a new principle in sensor design, *i.e.*, using triple-labeled pH nanosensors incorporating two pH-sensitive fluorophores and a reference fluorophore for ratiometric measurements of up to 4 pH units within one nanoparticle-based sensor. Furthermore, we have compared this sensor to conventional dual-labeled

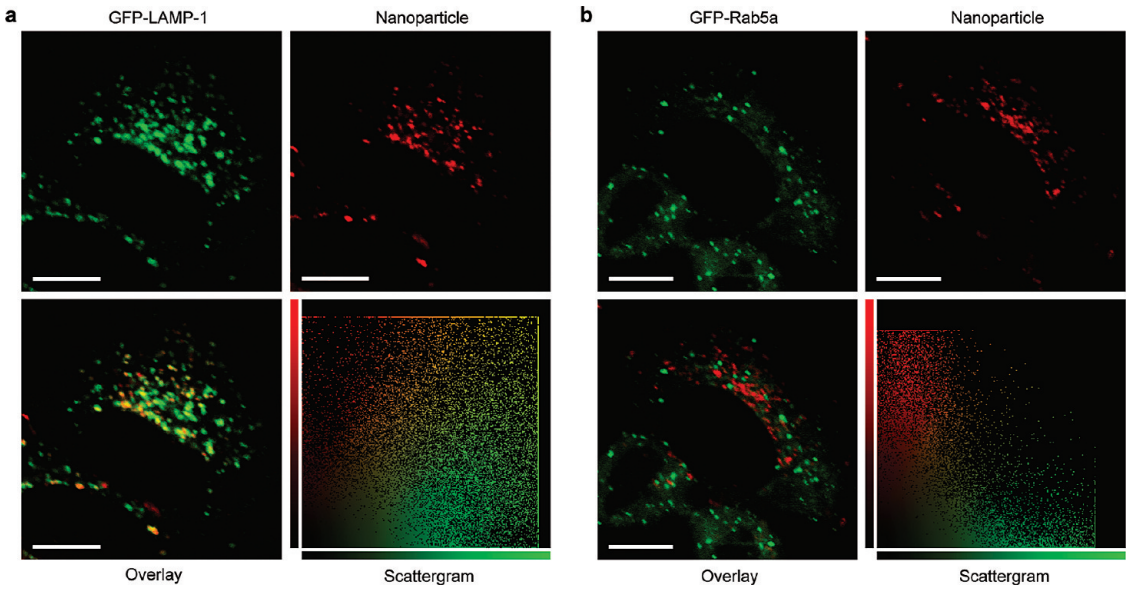

Figure 5. Localization of the nanosensor. Co-localization of (a) RhB-labeled nanoparticle with lysosomal marker GFP-LAMP-1 and (b) early endosomal marker GFP-Rab5a. HepG2 cells were tranduced with plasmids encoding GFP-tagged marker and incubated with nanoparticle for 24 h. Top left image: GFP tagged lysosomal/endosomal marker; top right: nanoparticle; bottom left: overlay; and bottom right: scattergram of all pixels in overlay relating green intensity to red intensity of the same pixel. Scale bar, 10 μm. Representative of three independent experiments.

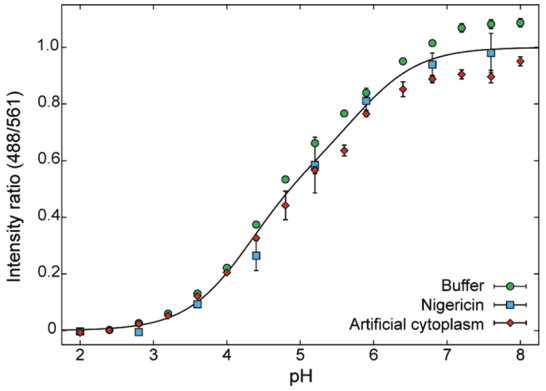

Figure 6. *In vitro* and *in situ* calibration of the triple-labeled nanosensor. Calibration was done in buffer, artificial cytoplasm, and inside cells. Ratiometric measurements of the nanosensor in different buffers are related to pH and fitted to eq 2 for triple-labeled nanosensors. The artificial cell cytoplasm was prepared by sonication of HeLa cells and mixed with buffers with controlled pH. *In situ* calibration was obtained by treatment of nanosensor-containing cells with nigericin in K^+-rich buffers. Normalization of ratios has been performed by subtraction of R_{min} and division by ($R_{max} - R_{min}$). Mean $\pm$ SD between three images are presented.

sensors. The triple-labeled sensor covers the physiologically relevant pH interval from 3.2 to 7.0 of the endosome–lysosome system. With this sensor, the pH was measured in the lysosomes, and the sensor can follow the rapid increase in pH up to 5.6 after treatment with the V-ATPase inhibitor bafilomycin A_1. The data obtained lie well within the sensitivity range of the triple-labeled sensor, ensuring reliable measurements. We demonstrate how these same measurements done with dual-labeled sensors have limitations, and their use can result in erroneous conclusions. In fact, a number of critical factors should be addressed before continuation to actual pH measurements with a nanosensor in cells. These factors include consideration of the measurable range of the sensor, appropriate performance of calibration (which should always be presented), appropriate background subtraction,[51] localization of the sensor in the cells, and finally cytotoxicity of the sensor.

Furthermore, we emphasize that the width of the distributions of ratios in a measurement is highly important. As seen in Figure 3, a measurement will always return a distribution of ratios around the mean value even for a homogeneous sample. This behavior has important implications. When the mean of the distribution approaches the R_{max}, part of the distribution actually exceeds the R_{max} and is thus not available for measurements of the pH. Ultimately, this renders the sensitive range of the sensor even smaller than the rule of thumb, $pK_a \pm 1$, as ratios start to fall out of the measurable range before the mean of the distributions is close to R_{max}. The width of a distribution of ratios is influenced by the natural distribution of pH in the cell; however, other factors also contribute. First, the amount of different fluorophores within the particles has a distribution; that is, the ratios of the amount of sensitive and reference fluorophores in the particles are distributed around a mean value, adding to the width of the overall distribution measured. More uniform particles will contribute less to this effect. Also, the scan speed necessary to obtain sufficient signal allows a small degree of particle diffusion and, in the worst case, a one-pixel movement between scanning at the two wavelengths, which ultimately changes the

ratio obtained in that pixel. This will contribute to a broadening of the distribution of measured ratios, but the effect can be reduced by averaging by using regions of interest or using pixel binning. Faster scanning leads to reduced signal intensity to noise ratios; hence, a compromise between the two has to be met for every experiment. In addition, the background noise also has a distribution, and even though a background subtraction is performed, this is subtracted as an average value, leaving the width of the distribution unchanged. Furthermore, the distribution of light from a point source (a particle), *i.e.*, the point spread function, contributes with different intensities of light to neighboring pixels, adding to the width of the distribution of measured ratios. Finally, nonsynchronized fluctuations of the lasers will also result in alterations of intensities and therefore contribute to a broadening of the distribution of ratios. Correction of laser intensity for each image can overcome this issue.

Despite the aforementioned challenges, the triple-labeled sensor extends the sensitive range considerably compared to a dual-labeled sensor and proves itself as a valuable tool for pH measurements of the endosomal–lysosomal system, where the measurements will reside well within the pH-sensitive range, ensuring easily interpretable and reliable measurements. The principle can even be expanded to include more sensor dyes, giving an even broader measurement range.

METHODS

Materials. Nigericin and bafilomycin A_1 were purchased from Sigma-Aldrich. For the BacMam virus transduction the Organelle Lights Lysosome-GFP and Organelle Lights Endosome-GFP were purchased from Invitrogen. Images were captured by a Leica TCS SP5 AOBS confocal microscope with a 63× water-immersed objective (Leica Microsystems, Germany). The microscope was equipped with an incubator box and CO_2 supply for optimal growth conditions during imaging (Life Imaging Services GmbH, Switzerland).

Characteristics of Employed Nanoparticles. Synthesis of cross-linked polyacrylamide nanoparticles is described in the Supporting Information. Characteristics of the employed nanoparticles are presented as their size and zeta potential as assayed by dynamic light scattering and phase analysis light scattering, respectively (ZetaPALS, Brookhaven, SE). Triple-labeled nanosensor: 57 nm and 4.6 mV. Dual-labeled nanosensor with Oregon Green: 61 nm and 7.8 mV. Fluorescein: 68 nm and 7.4 mV. Nanoparticle for co-localization: 110 nm and 50 mV.

Cell Culture. The HepG2 and HeLa cell lines were originally obtained from the American Type Culture Collection (ATCC) and maintained in Dulbecco's modified Eagle's medium supplemented with 10% fetal bovine serum (Sigma-Aldrich) and 100 UI/mL penicillin and streptomycin (Lonza). Cell cultures were incubated in a 5% CO_2 humidified incubator at 37 °C.

Calibration. *In vitro* calibration curves were generated from fluorescence images of the nanosensor at 12.5 or 25 mg/mL in 60 mM buffers (20 mM HEPES/20 mM MES/20 mM acetate/100 mM NaCl) from pH 2.1 to 8.2. For calibration in buffers with artificial cytoplasm, 10^6 HeLa cells per mL of Milli-Q water was sonicated for 1/2 h and mixed 1:2 with 120 mM buffers, pH was measured, and the solution was finally mixed with sensors in a 3:1 ratio for a final concentration of 60 mM buffer and 12.5 mg/mL nanosensor. The microscope was focused in a plane within the solution, and with the same settings (*e.g.*, laser power, gain, and resolution) as were employed for the imaging of corresponding cells with internalized nanosensor, images were taken with sequential excitation at 488 and 561 nm. A total of 450 ROIs, with the size of ROIs obtained on cell images, were drawn on every buffer image, and calibration curves are presented with mean ± SD. *In situ* calibration curves were generated by imaging cells with internalized nanosensor in high-K^+ buffers of known pH in the presence of nigericin. The same buffer system was used as for the *in vitro* calibration with the substitution of NaCl with KCl. HeLa cells were treated with 10 μg/mL nanosensor for 24 h as described, washed in appropriate pH clamp buffer, and then equilibrated in buffer containing 10 μg/mL nigericin for 20 min. Three images were acquired of three to seven cells each for every pH for quantitative ratiometric analysis.

Nanosensor Treatment and Image Acquisition. HepG2 cells were seeded in 35 mm culture dishes with a 10 mm microwell glass bottom for 24 h. Cells were incubated with 10 μg/mL nanosensor for 24 h (and 1.5 and 2 h for the kinetic study), washed three times with ice-cold phosphate-buffered saline (PBS) supplemented with heparin (20 units/mL), washed once with PBS, and kept in growth medium without phenol-red for observation by confocal microscopy. Images were collected by sequential line scanning, with excitation at 488 and 561 nm. Emission was collected by photomultiplier tubes in the ranges 498–570 and 571–735 nm, respectively, obtained by tunable high-reflectance mirrors. The microscope was equipped with an incubator box and CO_2 supply to ensure optimal growth conditions during microscopy. Cells vere imaged sequentially (by line) with excitation at 488 and 561 nm along with a DIC image. For bafilomycin A_1 analysis cells were first imaged in media and then, while on the microscope stage, supplemented with 50 nM bafilomycin A_1. The same cells were then imaged after 30 to 35 min.

Image Analysis. The background of every image series was determined by plotting a histogram with number of pixels per intensity level for both colors (Supporting Figure S1). The background level was identified as the main peak at low intensities, and the top of this peak was used as a measure of the background level for each color. This value was subtracted from all images in a series and the corresponding calibration curve. Two methods have been employed for the measurements of pH. The first method utilized the Fiji processing package based on ImageJ[34] for the generation of a mask with ROIs localizing the nanosensor-containing vesicles. The mask was generated by addition of the two corresponding intensity images (in order to include all nanosensor-containing vesicles), the image was thresholded to produce a binary image, and all regions larger than 0.15 μm^2 were recognized as ROIs. This mask was superimposed onto the original intensity images, and mean intensity for each ROI for each color was calculated. After background subtraction the intensity ratio of each ROI was converted to pH *via* the calibration curve. The second method was based on custom-made software where image preprocessing was utilized, including (i) binning of neighboring pixels (in order to eliminate artifacts caused by sensor diffusion in between scanning the two color channels), (ii) detection of sensor domains by comparison of the pixel intensity (of the reference dye) to the average intensity of the neighborhood (eliminate single pixels domains), and (iii) removal of pixels with reference dye intensity lower than a cutoff. The intensities of the included pixels were converted to pH *via* the calibration curve. pH histograms obtained from both methods were determined as averages based on 5–9 images.

Co-localization. HepG2 cells were seeded in 24-well plates on 9 mm cover glass slides for 24 h. They were then transduced

with Organelle Lights regents according to the manufacturer. Briefly, cells were washed in PBS and incubated with baculovirus (containing either GFP-Rab5a or GFP-LAMP-1 plasmids) diluted 1:1 to 1:6 in PBS for 4 h at room temperature with gentle shaking. Virus-containing solution were then aspirated and replaced with full growth medium supplemented with 0.1% BacMam enhancer. Cells were incubated at optimal growth conditions for 2 h, and medium was replaced with normal growth medium containing 10 μg/mL RhB-labeled nanoparticles and incubated overnight. This nanoparticle resembles the nanosensor without pH-sensitive fluorophores in order for co-localization with GFP-tagged markers. Cells were then washed as described for nanosensor treatment and imaged by confocal microscopy with excitation at 488 and 561 nm. After appropriate background subtraction the correlation coefficients—Pearson's correlation coefficient and an overlap coefficient—were calculated.

Acknowledgment. This work was financially supported by Kræftens Bekæmpelse, Denmark, and the Danish Council for Independent Research (Technology and Production Sciences (FTP) grant no. (LiMeS) 274-07-0172).

Supporting Information Available: Detailed description of synthetic procedure of nanosensor preparation and derivations of pH equations. Furthermore, determination of background levels of images, comparison of image processing methods, temporal pH measurements following bafilomycin A_1 treatment, distributions of measurements, co-localization of a neutral nanoparticle with lysosomes, cytotoxicity of nanosensor, and calibration of the triple-labeled nanosensor in buffer. This material is available free of charge *via* the Internet at http://pubs.acs.org.

REFERENCES AND NOTES

1. Casey, J. R.; Grinstein, S.; Orlowski, J. Sensors and Regulators of Intracellular pH. *Nat. Rev. Mol. Cell Biol.* **2010**, *11*, 50–61.
2. Whitten, S. T.; Garcia-Moreno, E. B.; Hilser, V. J. Local Conformational Fluctuations can Modulate the Coupling between Proton Binding and Global Structural Transitions in Proteins. *Proc. Natl. Acad. Sci. U. S. A.* **2005**, *102*, 4282–4287.
3. Kornak, U.; Reynders, E.; Dimopoulou, A.; van Reeuwijk, J.; Fischer, B.; Rajab, A.; Budde, B.; Nurnberg, P.; Foulquier, F. ARCL Debre-type Study Group.; *et al.* Impaired Glycosylation and Cutis Laxa Caused by Mutations in the Vesicular H+-ATPase Subunit ATP6V0A2. *Nat. Genet.* **2008**, *40*, 32–34.
4. Pouyssegur, J.; Sardet, C.; Franchi, A.; L'Allemain, G.; Paris, S. A Specific Mutation Abolishing Na+/H+ Antiport Activity in Hamster Fibroblasts Precludes Growth at Neutral and Acidic pH. *Proc. Natl. Acad. Sci. U. S. A.* **1984**, *81*, 4833–4837.
5. Thangaraju, M.; Sharma, K.; Liu, D.; Shen, S. H.; Srikant, C. B. Interdependent Regulation of Intracellular Acidification and SHP-1 in Apoptosis. *Cancer Res.* **1999**, *59*, 1649–1654.
6. Andresen, T. L.; Jensen, S. S.; Jorgensen, K. Advanced Strategies in Liposomal Cancer Therapy: Problems and Prospects of Active and Tumor Specific Drug Release. *Prog. Lipid Res.* **2005**, *44*, 68–97.
7. Jolck, R. I.; Feldborg, L. N.; Andersen, S.; Moghimi, S. M.; Andresen, T. L. Engineering Liposomes and Nanoparticles for Biological Targeting. *Adv. Biochem. Eng. Biotechnol.* **2010**, DOI: 10.1007/10_2010_92.
8. Bach, G.; Chen, C. S.; Pagano, R. E. Elevated Lysosomal pH in Mucolipidosis Type IV Cells. *Clin. Chim. Acta* **1999**, *280*, 173–179.
9. Hara-Chikuma, M.; Wang, Y.; Guggino, S. E.; Guggino, W. B.; Verkman, A. S. Impaired Acidification in Early Endosomes of ClC-5 Deficient Proximal Tubule. *Biochem. Biophys. Res. Commun.* **2005**, *329*, 941–946.
10. Ji, J.; Rosenzweig, N.; Griffin, C.; Rosenzweig, Z. Synthesis and Application of Submicrometer Fluorescence Sensing Particles for Lysosomal pH Measurements in Murine Macrophages. *Anal. Chem.* **2000**, *72*, 3497–3503.
11. Modi, S.; M, G. S.; Goswami, D.; Gupta, G. D.; Mayor, S.; Krishnan, Y. A DNA Nanomachine that Maps Spatial and Temporal pH Changes Inside Living Cells. *Nat. Nanotechnol.* **2009**, *4*, 325–330.
12. Overly, C. C.; Lee, K. D.; Berthiaume, E.; Hollenbeck, P. J. Quantitative Measurement of Intraorganelle pH in the Endosomal-Lysosomal Pathway in Neurons by Using Ratiometric Imaging with Pyranine. *Proc. Natl. Acad. Sci. U. S. A.* **1995**, *92*, 3156–3160.
13. Tycko, B.; Keith, C. H.; Maxfield, F. R. Rapid Acidification of Endocytic Vesicles Containing Asialoglycoprotein in Cells of a Human Hepatoma Line. *J. Cell Biol.* **1983**, *97*, 1762–1776.
14. van Weert, A. W.; Dunn, K. W.; Gueze, H. J.; Maxfield, F. R.; Stoorvogel, W. Transport from Late Endosomes to Lysosomes, but Not Sorting of Integral Membrane Proteins in Endosomes, Depends on the Vacuolar Proton Pump. *J. Cell Biol.* **1995**, *130*, 821–834.
15. Bradley, M.; Alexander, L.; Duncan, K.; Chennaoui, M.; Jones, A. C.; Sanchez-Martin, R. M. PH Sensing in Living Cells Using Fluorescent Microspheres. *Bioorg. Med. Chem. Lett.* **2008**, *18*, 313–317.
16. Chen, Q. R.; Zhang, L.; Luther, P. W.; Mixson, A. J. Optimal Transfection with the HK Polymer Depends on its Degree of Branching and the pH of Endocytic Vesicles. *Nucleic Acids Res.* **2002**, *30*, 1338–1345.
17. Schreiber, R.; Zhang, F.; Haussinger, D. Regulation of Vesicular pH in Liver Macrophages and Parenchymal Cells by Ammonia and Anisotonicity as Assessed by Fluorescein Isothiocyanate-Dextran Fluorescence. *Biochem. J.* **1996**, *315*), 385–392.
18. Peng, J.; He, X.; Wang, K.; Tan, W.; Wang, Y.; Liu, Y. Noninvasive Monitoring of Intracellular pH Change Induced by Drug Stimulation Using Silica Nanoparticle Sensors. *Anal. Bioanal Chem.* **2007**, *388*, 645–654.
19. Csernoch, L.; Bernengo, J. C.; Szentesi, P.; Jacquemond, V. Measurements of Intracellular Mg^{2+} Concentration in Mouse Skeletal Muscle Fibers with the Fluorescent Indicator Mag-Indo-1. *Biophys. J.* **1998**, *75*, 957–967.
20. Graefe, A.; Stanca, S. E.; Nietzsche, S.; Kubicova, L.; Beckert, R.; Biskup, C.; Mohr, G. J. Development and Critical Evaluation of Fluorescent Chloride Nanosensors. *Anal. Chem.* **2008**, *80*, 6526–6531.
21. Grynkiewicz, G.; Poenie, M.; Tsien, R. Y. A New Generation of Ca^{2+} Indicators with Greatly Improved Fluorescence Properties. *J. Biol. Chem.* **1985**, *260*, 3440–3450.
22. Koo, Y. E.; Cao, Y.; Kopelman, R.; Koo, S. M.; Brasuel, M.; Philbert, M. A. Real-Time Measurements of Dissolved Oxygen Inside Live Cells by Organically Modified Silicate Fluorescent Nanosensors. *Anal. Chem.* **2004**, *76*, 2498–2505.
23. Ruedas-Rama, M. J.; Hall, E. A. K^+-Selective Nanospheres: Maximising Response Range and Minimising Response Time. *Analyst* **2006**, *131*, 1282–1291.
24. Sumner, J. P.; Aylott, J. W.; Monson, E.; Kopelman, R. A Fluorescent PEBBLE Nanosensor for Intracellular Free Zinc. *Analyst* **2002**, *127*, 11–16.
25. Clark, H. A.; Kopelman, R.; Tjalkens, R.; Philbert, M. A. Optical Nanosensors for Chemical Analysis Inside Single Living Cells. 2. Sensors for pH and Calcium and the Intracellular Application of PEBBLE Sensors. *Anal. Chem.* **1999**, *71*, 4837–4843.
26. Doussineau, T.; Trupp, S.; Mohr, G. J. Ratiometric pH-Nanosensors Based on Rhodamine-Doped Silica Nanoparticles Functionalized with a Naphthalimide Derivative. *J. Colloid Interface Sci.* **2009**, *339*, 266–270.
27. Hornig, S.; Biskup, C.; Graefe, A.; Wotschadlo, J.; Liebert, T.; Mohr, G. J.; Heinze, T. Biocompatible Fluorescent Nanoparticles for pH-Sensoring. *Soft Matter* **2008**, *4*, 1169–1172.
28. Schulz, A.; Wotschadlo, J.; Heinze, T.; Mohr, G. J. Fluorescent Nanoparticles for Ratiometric pH-Monitoring in the Neutral Range. *J. Mater. Chem.* **2010**, *20*, 1475–1482.

29. Buck, S. M.; Xu, H.; Brasuel, M.; Philbert, M. A.; Kopelman, R. Nanoscale Probes Encapsulated by Biologically Localized Embedding (PEBBLEs) for Ion Sensing and Imaging in Live Cells. *Talanta* **2004**, *63*, 41–59.
30. Ohkuma, S.; Poole, B. Fluorescence Probe Measurement of the Intralysosomal pH in Living Cells and the Perturbation of pH by Various Agents. *Proc. Natl. Acad. Sci. U. S. A.* **1978**, *75*, 3327–3331.
31. Thomas, J. A.; Buchsbaum, R. N.; Zimniak, A.; Racker, E. Intracellular pH Measurements in Ehrlich Ascites Tumor Cells Utilizing Spectroscopic Probes Generated in Situ. *Biochemistry* **1979**, *18*, 2210–2218.
32. Downey, G. P.; Botelho, R. J.; Butler, J. R.; Moltyaner, Y.; Chien, P.; Schreiber, A. D.; Grinstein, S. Phagosomal Maturation, Acidification, and Inhibition of Bacterial Growth in Nonphagocytic Cells Transfected with FcgammaRIIA Receptors. *J. Biol. Chem.* **1999**, *274*, 28436–28444.
33. Sun, H.; Almdal, K.; Andresen, T. L. Expanding the Dynamic Measurement Range for Polymeric Nanoparticle pH Sensors. *Chem. Commun. (Cambridge)* **2011**, *47*, 5268–5270.
34. Sun, H.; Andresen, T. L.; Benjaminsen, R. V.; Almdal, K. Polymeric Nanosensors for Measuring the Full Dynamic pH Range of Endosomes and Lysosomes in Mammalian Cells. *J. Biomed. Nanotechnol.* **2009**, *5*, 676–682.
35. Clark, H. A.; Hoyer, M.; Philbert, M. A.; Kopelman, R. Optical Nanosensors for Chemical Analysis Inside Single Living Cells. 1. Fabrication, Characterization, and Methods for Intracellular Delivery of PEBBLE Sensors. *Anal. Chem.* **1999**, *71*, 4831–4836.
36. Bizzarri, R.; Arcangeli, C.; Arosio, D.; Ricci, F.; Faraci, P.; Cardarelli, F.; Beltram, F. Development of a Novel GFP-Based Ratiometric Excitation and Emission pH Indicator for Intracellular Studies. *Biophys. J.* **2006**, *90*, 3300–3314.
37. Llopis, J.; McCaffery, J. M.; Miyawaki, A.; Farquhar, M. G.; Tsien, R. Y. Measurement of Cytosolic, Mitochondrial, and Golgi pH in Single Living Cells with Green Fluorescent Proteins. *Proc. Natl. Acad. Sci. U. S. A.* **1998**, *95*, 6803–6808.
38. Abràmoff, M. D.; Magalhães, P. J.; Ram, S. J.; Abràmoff, M. D.; Magalhães, P. J.; Ram, S. J. Image Processing with imageJ. *Biophoton. Int.* **2004**, *11*, 36–41.
39. Forgac, M. Vacuolar ATPases: Rotary Proton Pumps in Physiology and Pathophysiology. *Nat. Rev. Mol. Cell Biol.* **2007**, *8*, 917–929.
40. Bowman, E. J.; Siebers, A.; Altendorf, K. Bafilomycins: A Class of Inhibitors of Membrane ATPases from Microorganisms, Animal Cells, and Plant Cells. *Proc. Natl. Acad. Sci. U. S. A.* **1988**, *85*, 7972–7976.
41. Hanada, H.; Moriyama, Y.; Maeda, M.; Futai, M. Kinetic Studies of Chromaffin Granule H^+-ATPase and Effects of Bafilomycin A1. *Biochem. Biophys. Res. Commun.* **1990**, *170*, 873–878.
42. Yoshimori, T.; Yamamoto, A.; Moriyama, Y.; Futai, M.; Tashiro, Y. Bafilomycin A1, a Specific Inhibitor of Vacuolar-Type H(+)-ATPase, Inhibits Acidification and Protein Degradation in Lysosomes of Cultured Cells. *J. Biol. Chem.* **1991**, *266*, 17707–17712.
43. Liao, C. W.; Lien, C. C. Estimating Intracellular Ca^{2+} Concentrations and Buffering in a Dendritic Inhibitory Hippocampal Interneuron. *Neuroscience* **2009**, *164*, 1701–1711.
44. Lewis, V.; Green, S. A.; Marsh, M.; Vihko, P.; Helenius, A.; Mellman, I. Glycoproteins of the Lysosomal Membrane. *J. Cell Biol.* **1985**, *100*, 1839–1847.
45. Kost, T. A.; Condreay, J. P.; Jarvis, D. L. Baculovirus as Versatile Vectors for Protein Expression in Insect and Mammalian Cells. *Nat. Biotechnol.* **2005**, *23*, 567–575.
46. Falcon-Perez, J. M.; Nazarian, R.; Sabatti, C.; Dell'Angelica, E. C. Distribution and Dynamics of Lamp1-Containing Endocytic Organelles in Fibroblasts Deficient in BLOC-3. *J. Cell. Sci.* **2005**, *118*, 5243–5255.
47. Manders, E. M. M.; Verbeek, F. J.; Aten, J. A. Measurement of Colocalization of Objects in Dual-Color Confocal Images. *J. Microsc. (Oxford, U.K.)* **1993**, *169*, 375–382.
48. Smallcombe, A. Multicolor Imaging: The Important Question of Co-Localization. *BioTechniques* **2001**, *30*), 1244–6.
49. Chavrier, P.; Parton, R. G.; Hauri, H. P.; Simons, K.; Zerial, M. Localization of Low Molecular Weight GTP Binding Proteins to Exocytic and Endocytic Compartments. *Cell* **1990**, *62*, 317–329.
50. Roberts, R. L.; Barbieri, M. A.; Ullrich, J.; Stahl, P. D. Dynamics of rab5 Activation in Endocytosis and Phagocytosis. *J. Leukoc. Biol.* **2000**, *68*, 627–632.
51. Broder, J.; Majumder, A.; Porter, E.; Srinivasamoorthy, G.; Keith, C.; Lauderdale, J.; Sornborger, A. Estimating Weak Ratiometric Signals in Imaging Data. I. Dual-Channel Data. *J. Opt. Soc. Am. A* **2007**, *24*, 2921–2931.